Supplementary Information

DFG-out Mode of Inhibition by an Irreversible type-1 Inhibitor Capable of Overcoming Gate-Keeper Mutations in FGF Receptors

Zhifeng Huang, Li Tan, Huiyan Wang, Yang Liu, Steven Blais, Jingjing Deng, Thomas Neubert, Nathanael S. Gray, Xiaokun Li, Moosa Mohammadi

Figure S1

A

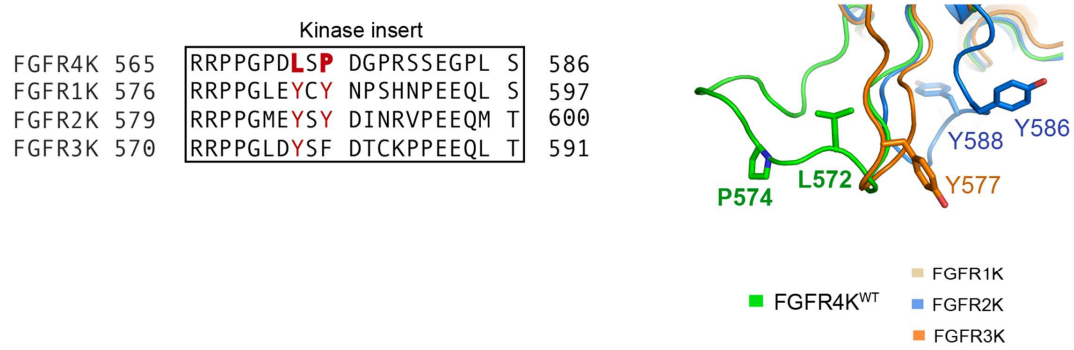

B

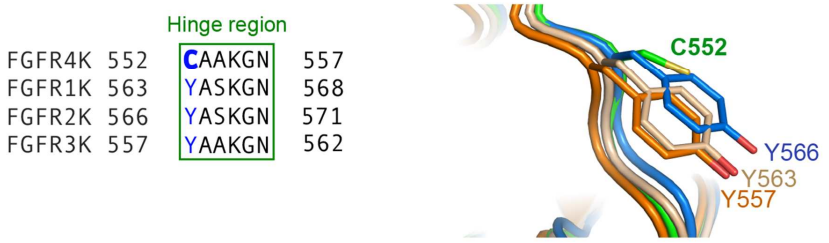

C

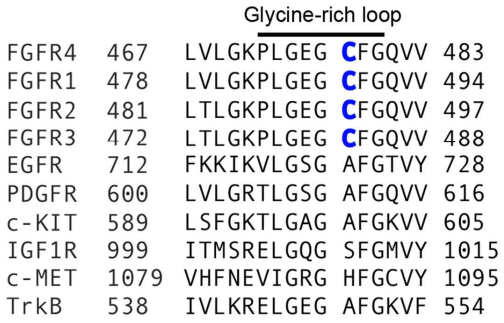

Supplementary Figure S1. Sequence alignment and structural superimposition of the kinase insert (**A**), hinge region (**B**) of FGFR1K (PDB ID: 3KY2[1], in wheat), FGFR2K (PDB ID: 2PVF [2], in blue), FGFR3K^{K650E} (PDB ID: 4K33[3], in orange) and FGFR4K (PDB ID: 4QQT, in green).Side chains of selected residues are shown as sticks and atom colorings are as follows: oxygens in red, nitrogens in blue, and coloring of carbons follow the coloring scheme of the kinases to which they belong. (**C**) Sequence alignment ofthe glycine-rich loops of FGFR1-4 and several RTKs

belonging to different RTK subfamilies including EGFR, PDGFR, c-KIT, IGF1R, c-MET and TrkB.

Figure S2

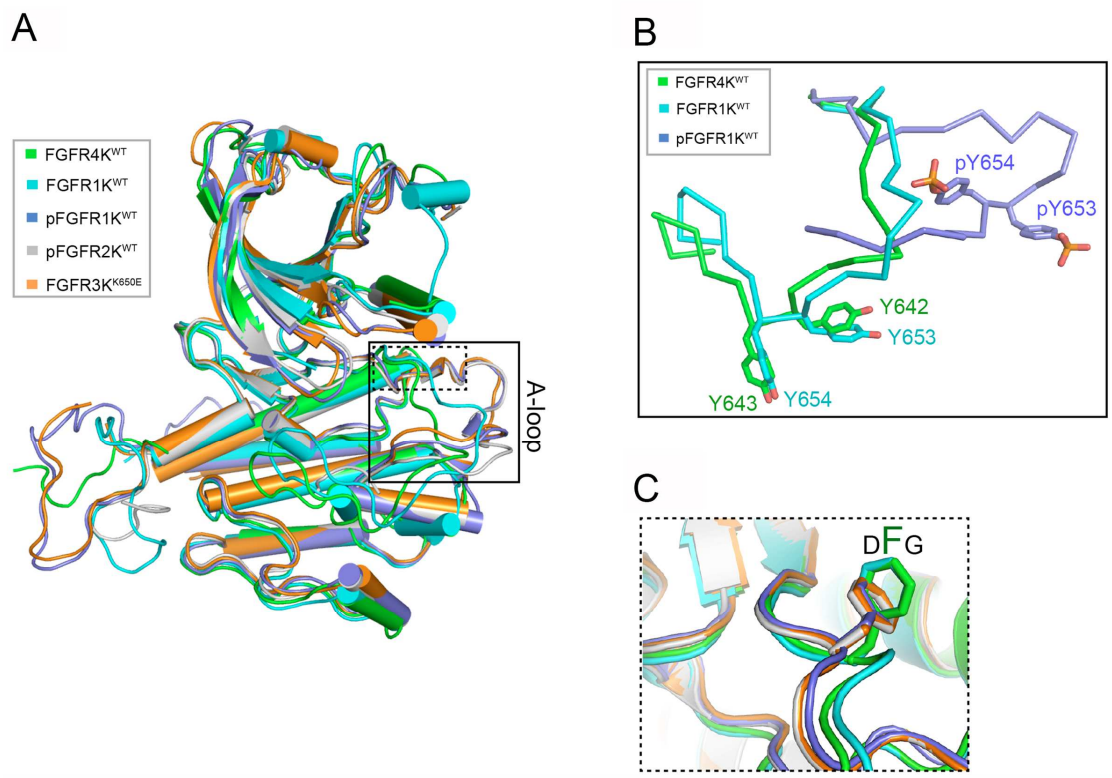

Supplementary Figure S2. Superimposition of wild-type FGFR4K with other FGFRK structures. (**A**)Superimposition of the wild-type FGFR4K structure (PDB ID: 4QQT, ingreen) ontothe structures of the unphosphorylated (PDB ID: 3KY2[1], in cyan) and phosphorylated (PDB ID: 3GQI[4], in lightblue) wild-type FGFR1K, the phosphorylated wild-type FGFR2K (PDB ID: 2PVF [2], in gray) and FGFR3^{K650E} (PDB ID: 4K33[3])structures. (**B**) The conformation of FGFR4K A-loop is very similar to that of the unphosphorylated autoinhibited FGFR1K. Side chains of A-loop tyrosines are shown as sticks and atom colorings are as follows: oxygens in red, nitrogens in blue,

and coloring of carbons follow the coloring scheme of the specific kinases. (**C**) As in FGFR1-3 kinase, the DFG motif of FGFR4K at the beginning of the A-loop adopts an "in" conformation.

Figure S3

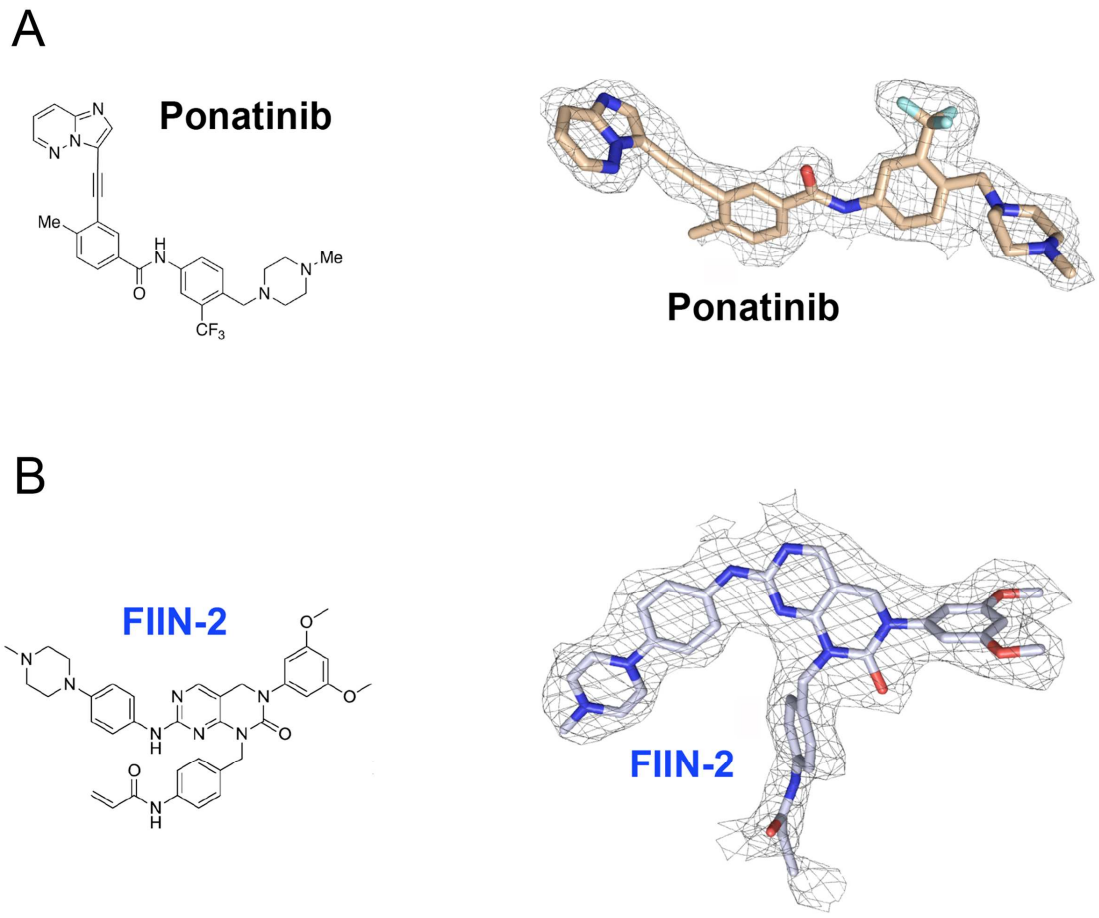

Supplementary Figure S3. The chemical structure of Ponatinib (**A**) and FIIN-2(**B**). Experimental electron density maps contoured at 2σ around the ponatinib (**A**, right panel) and FIIN-2 (**B**, right panel).

Figure S4

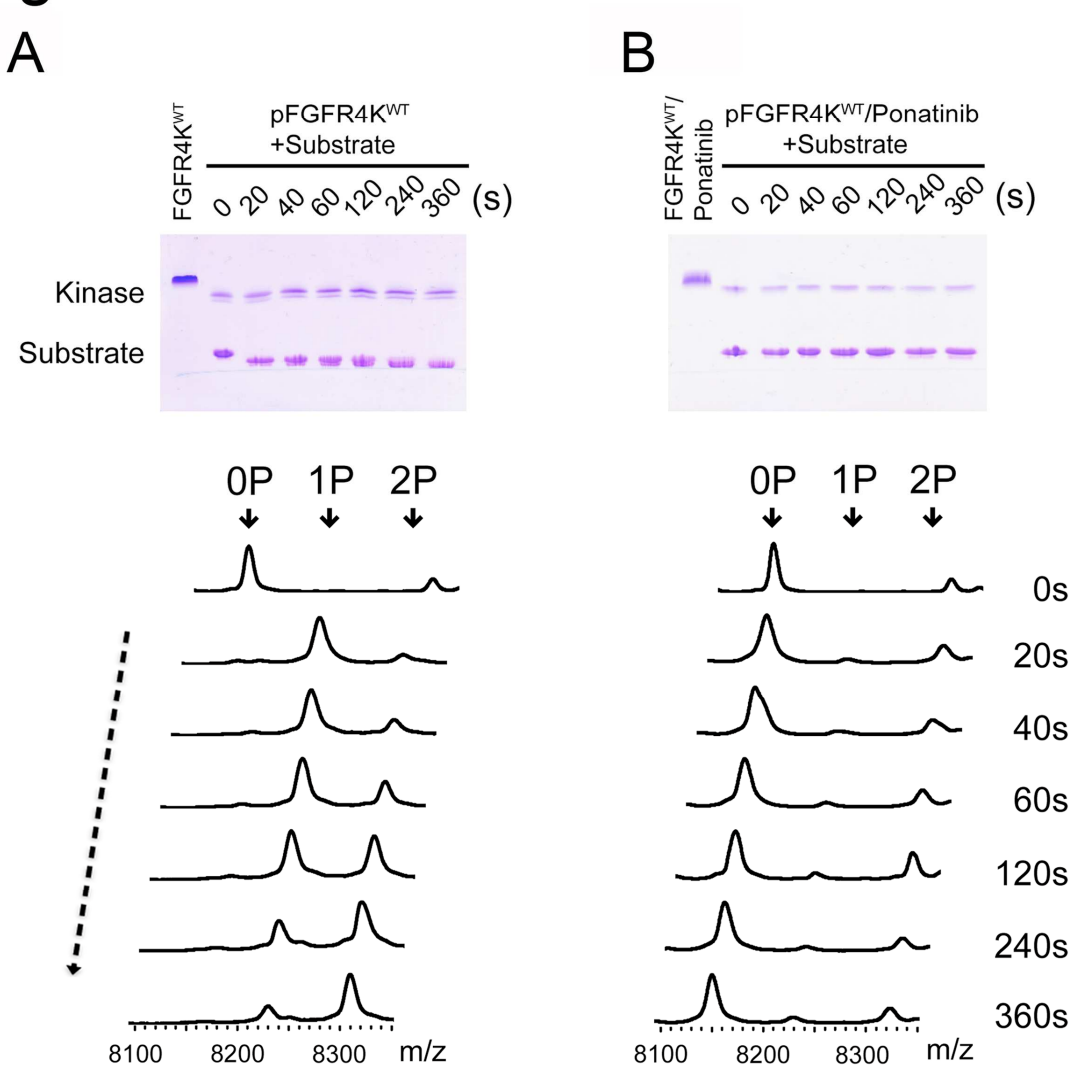

Supplementary Figure S4. Ponatinib is capable of inhibiting phosphorylated activated wild-type FGFR4K. Thetime course of substrate phosphorylation by pFGFR4K^{WT} in the absence (**A**) and presence of ponatinib (1:2) (**B**) were compared using native-PAGE (upper panel) coupled with time-resolved MALDI-TOF MS (lower panel**)**.

Figure S5

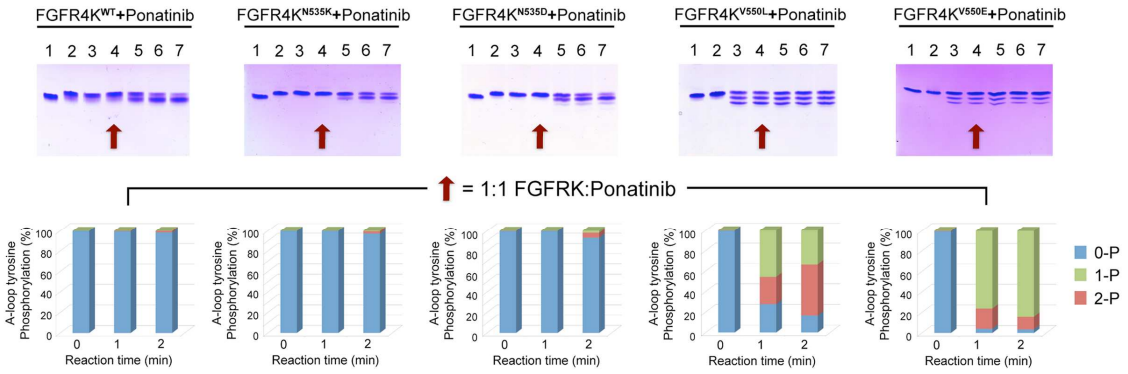

Supplementary Figure S5. The FGFR4K^{V550L} and FGFR4K^{V550E} gate-keeper mutants are refractory to inhibition by Ponatinib.Native-PAGE and LC-MS/MSanalysis of A-loop tyrosine phosphorylation in FGFR4K^{WT},FGFR4K^{N535K}, FGFR4K^{N535D}, FGFR4K^{V550L} and FGFR4K^{V550E} after 1 min autophosphorylation reaction in the presence (lanes 3-6) and absence of ponatinib (lane 7).The kinase:inhibitor molar ratios in lanes 3-7 are1:2, 1:1, 1:0.5, 1:0.2, and 1:0 respectively. The control lanes 1 and 2 are kinase alone and 1:1 mixture of kinase with Ponatinib. The red arrow indicates the inhibition achieved at 1:1 kinase:ponatinib molar ratio.

Figure S6

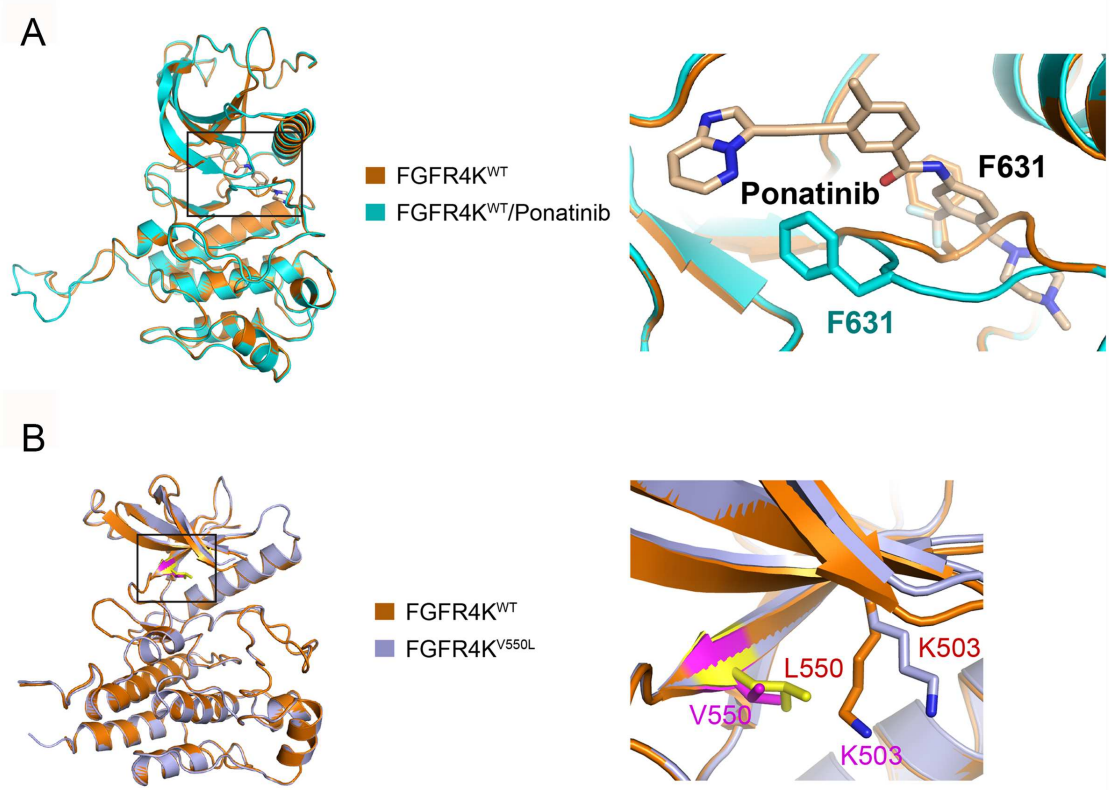

Supplementary Figure S6. Superimposition of FGFR4K^{WT} (PDB ID:4QQT, in orange) onto FGFR4K-ponatinib complex (PDB ID: 4QRC, in cyan)and FGFR4K^{V550L}(PDB ID: 4QQJ, in lightblue).(**A**)Ponatinib forces the DFG region out of the ATP binding pocket.Ponatinib is rendered as sticks and labeled in black. The phenylalaninein DFG region of FGFR4K^{WT} and FGFR4K^{WT}-ponatinib complex are rendered as orange and cyan sticks, and labeled in black and cyan, respectively.(**B**)The FGFR4K^{WT}andFGFR4K^{V550L} structures are completely superimposable with the exception of the side chain of catalytic Lys-503, which is displaced to make room for the larger aliphatic side chain of Leu-550. TheV550 and K503 in FGFR4K^{WT}are labeled in pink, and L550 and K503 in FGFR4K^{V550L} are labeled red.

Figure S7

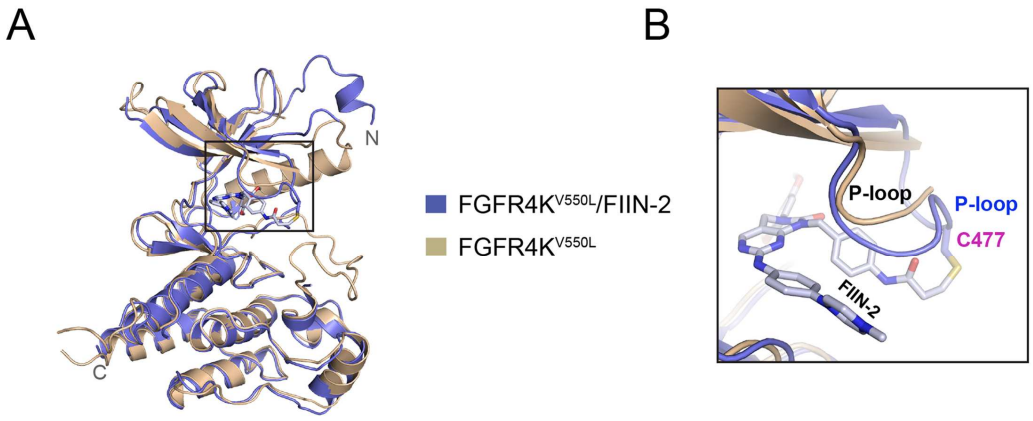

Supplementary Figure S7. The crystal structure of FGFR4K^{V550L} in complex with FIIN-2. **(A)**Superimposition of FGFR4K^{V550L} (PDB ID: 4QQJ, inwheat) ontoFGFR4K^{V550L}-FIIN-2 complex (PDB ID: 4QQ5, inblue).(**B**) The glycine-rich loop in FGFR4K^{V550L}-FIIN-2 undergoes a major conformational change in response to drug binding. The FIIN-2 is rendered as sticks and labeled in black.

SUPPLEMENTARY METHODS

Protein expression and purification

cDNA fragment encoding residues L445 to E753(FGFR4K$^{445\text{-}753}$) of human FGFR4 (Accession code: AEO19723.1) was amplified by PCR, and subcloned into NcoI and Hind III restrictions sites of a pET bacterial expression vector in frame with an N-terminal 6XHis-tag to aid in protein purification. To circumvent disulfide-linked dimerization, in the FGFR4K$^{445\text{-}753}$ construct, cysteine 477 in the glycine-rich loop of the kinase was mutated to alanine. This construct served as the template to introduce the N535K, N535D, V550L and V550E pathogenic mutations (FGFR4K^{N535K}, FGFR4K^{N535D}, FGFR4K^{V550L}, FGFR4K^{V550E}). Additionally, for the crystallization of FGFR4K in complex with the irreversible kinase inhibitor (FIIN-2), the A477 was reverted back to cysteine in FGFR4K^{V550L} (FGFR4K$^{V550L/C477}$). All the mutations were introduced using the QuikChange site-directed mutagenesis kit (Stratagene). The bacterial strain BL21(DE3) cells were transformed with the expression constructs, and kinase expression was induced with 1 mM isopropyl-L-thio-B-D-galactopyranoside (IPTG) overnight at 16-25 °C depending on the construct. The cells were then lysed using the Emulsiflex-C3 (Avestin, Inc.) high volume homogenizer, and the soluble kinase proteins were purified using sequential Ni^{2+} chelating and anion exchange chromatography(Souce Q, GE Healthcare Life Sciences). Traces of phosphorylation on wild-type and mutant kinases were removed by treating the proteins with FastAP™ Thermosensitive Alkaline Phosphatase (Thermo Scientific) and kinases were re-purified by anion exchange chromatography (Mono Q, GE Healthcare Life Sciences). To make homogeneously

phosphorylated FGFR4K, sample wild-type FGFR4K ($FGFR4K^{WT}$) was mixed with ATP and $MgCl_2$ at room temperature. The reaction concentrations of the kinase, ATP and $MgCl_2$ were 100 mM, 20 mM and 40 mM, respectively. The reaction was quenched by adding EDTA to a final concentration of 50 mM and the reaction mixture was loaded onto Sizing-75 column. Homogeneously phosphorylated $FGFR4K^{WT}$was then purified by Mono Q chromatography. The C-terminal tail peptide of FGFR2 (residues L761 to T821, $FGFR2K^{761-821}$), which contains five authentic tyrosine phosphorylation sites (Y769, Y779, Y783, Y805 and Y812), was expressed and purified using sequential Ni^{2+} chelating and size exclusion chromatography. The purity of the proteins was estimated to be >98% based on SDS-PAGE analysis.

Crystallization and structure determination

All the crystals were grown by hanging drop vapor diffusion method either at 4°C ($FGFR4K^{WT}$, $FGFR4K^{V550L}$, and $FGFR4K^{WT}$-Ponatinib) or 18°C ($FGFR4K^{V550L/Cys477}$-FIIN-2). Purified $FGFR4K^{WT}$ and $FGFR4K^{V550L}$ proteins were concentrated to ~20 mg/mL using Centricon-10 (Millipore), and were mixed with the ATP-analogue (AMP-PCP) and $MgCl_2$ at a molar ratio of 1:3:15. $FGFR4K^{WT}$ crystallized in a buffer composed of 0.1 M MES (pH 5.5), 20% (w/v) PEG 4000, 0.2 M Li_2SO_4 and 0.01 M Taurine. Crystals of the $FGFR4K^{V550L}$ were obtained using crystallization buffer composed of 0.1 M Tris (pH 7.5), 20% (w/v) PEG 1500 and 0.2 M $(NH_4)_2SO_4$. To generate $FGFR4K^{WT}$-Ponatinib co-crystals, $FGFR4K^{WT}$ and ponatinib were mixed at a molar ratio of 1:1.2 and crystallized using crystallization buffer composed of 0.1 M MES (pH 5.5), 25% (w/v) PEG 4000, 0.15 M $(NH_4)_2SO_4$ and 4% (v/v) Formamide. To

generate co-crystals of the FGFR4K$^{V550L/Cys477}$ with FIIN-2, kinase and FIIN-2 were mixed at a molar ratio of 1:1.2 and incubated at 4 °C overnight to allow for covalent bond formation between the compound and cysteine 477 in the kinase glycine-rich loop. FGFR4K$^{V550L/C477}$-FIIN-2 complex was crystallized using crystallization buffer composed of 0.1 M HEPES (pH 7.5), 1.0~1.2 M $(NH_4)_2SO_4$ and 10 mM Yttrium (III) chloride hexahydrate. Crystals grew in about 7-15 days and were stabilized in mother liquor by stepwise increasing glycerol concentration to 25%, and then flash-frozen in liquid nitrogen. Diffraction data were collected at Beamline X-4C at the National Synchrotron Light Source, Brookhaven National Laboratory. All diffraction data were processed using *HKL2000* Suite [5]. All the crystal structures were solved using maximum likelihood molecular replacement program *Phaser* in *PHENIX* software suite[6]. The crystal structure of wild-type FGFR2 kinase (PDB ID: 2PSQ) [2]was used as the search model. The A-loop, the b2-b3 loop and kinase insert region were removed from the search model. Model building was carried out using *Coot*[7], and refinements were done using *phenix.refine* in *PHENIX suite* [6]. Data collection and structure refinement statistics are listed in **Table 1**. Atomic superimpositions were performed using program *lsqkab*[8] in *CCP4 Suite*[9]and structural representations were prepared using *PyMol*[10].

Peptide substrate phosphorylation assay by native gel and MALDI-TOF Mass spectrometry

Peptide substrate phosphorylation assays were performed by adding wild-type and pathogenic mutated FGFR4 kinases (FGFR4K^{WT}, FGFR4K^{N535K}, FGFR4K^{N535D},

FGFR4K^{V550L}, FGFR4K^{V550E}) to the reaction solution containing the FGFR2 kinase peptide substrate (FGFR2K$^{761-821}$), ATP and $MgCl_2$ at room temperature. The final concentrations of the enzyme, substrate, ATP, and $MgCl_2$ were 13.5 μM, 262 μM, 10 mM, and 20 mM, respectively. The reactions were quenched at different time points by adding EDTA to a final concentration of 33.33 mM. Tyrosine phosphorylation of the substrate peptide at different time points was monitored by native gel electrophoresis and quantified using mass spectrometry. Briefly, all reaction samples were diluted 15 times with 0.1% TFA and analyzed by positive ion MALDI-TOF MS (Bruker Autoflex MALDI-TOF, Bruker Daltonics) in linear mode. For each sample, ion signals from 500 laser shots were combined into one mass spectrum. After spectrum smoothing and background subtraction, the ion count peak heights from the unphosphorylated substrate and its phosphorylated versions were used for relative quantification of substrate phosphorylation.

To examine the inhibitory efficiency of ponatinib or FIIN-2, the kinases were complexed with the compounds in 1:1 molar ratio, and the complexes were added to the reaction buffer containing the peptide substrate (FGFR2K$^{761-821}$), ATP and $MgCl_2$ at room temperature. The final concentrations of the kinase-inhibitor complex, substrate, ATP, and $MgCl_2$ were 13.5 μM, 262 μM, 20 mM, and 40 mM, respectively. The reactions were quenched at different time points by adding EDTA to a final concentration of 50 mM. Tyrosine phosphorylation of the peptide at different time points was analyzed by native gel electrophoresis and quantified by mass spectrometry as described above.

Inhibition of kinase autophosphorylation by ponatinib

The wild-type FGFR4 kinase and its pathogenic variants ($FGFR4K^{WT}$, $FGFR4K^{N535K}$, $FGFR4K^{N535D}$, $FGFR4K^{V550L}$, $FGFR4K^{V550E}$) were added into reaction solutions containing ATP,$MgCl_2$, and increasing concentrations of Ponatinib at room temperature. The final concentrations of kinase, ATP, and $MgCl_2$were 40 μM, 20 mM,and 40 mM, respectively. The molar ratios of kinase/inhibitor inthe reaction mix were 1:2, 1:1, 1:0.5, 1:0.2. Following 1 and 2 min incubation, the reactionswere quenched by adding EDTA to a final concentration of 50 mM, and kinase autophosphorylation/inhibition was monitored by native gel electrophoresis. For mass spectrometric analysis, 2 μL sample were mixed with 6 μL 12.5 mM ammonium bicarbonate, and heated to 95 °C for 5 minutes. Following cooling to room temperature, 2 μL of 0.1 μg/μL trypsin solution (Trypsin Gold, Promega) was added to each sample and the samples were digested in a microwave oven for 2 min with 1L of water present to buffer the energy. Finally, 2 μL digested sample was added to 18 μL 0.1% formic acid and analyzed by LTQ Orbitrap (Thermo Electron) LC-MS/MS. The ion counts from the phosphopeptide containing A-loop tyrosines and its unphosphorylated version were extracted from the most intense monoisotopic mass/charge peaks and were used to estimate the ratio of phosphorylation on tyrosines.

SUPPLEMENTARY REFERENCES

1. Bae, J. H., Boggon, T. J., Tome, F., Mandiyan, V., Lax, I., and Schlessinger, J. (2010) Asymmetric receptor contact is required for tyrosine autophosphorylation of fibroblast growth factor receptor in living cells, *Proc. Natl. Acad. Sci. U. S. A. 107*, 2866-2871.
2. Chen, H., Ma, J., Li, W., Eliseenkova, A. V., Xu, C., Neubert, T. A., Miller, W. T., and Mohammadi, M. (2007) A molecular brake in the kinase hinge region regulates the activity of receptor tyrosine kinases, *Mol. Cell 27*, 717-730.
3. Huang, Z., Chen, H., Blais, S., Neubert, T. A., Li, X., and Mohammadi, M. (2013) Structural mimicry of a-loop tyrosine phosphorylation by a pathogenic FGF receptor 3 mutation, *Structure 21*, 1889-1896.
4. Bae, J. H., Lew, E. D., Yuzawa, S., Tome, F., Lax, I., and Schlessinger, J. (2009) The Selectivity of Receptor Tyrosine Kinase Signaling Is Controlled by a Secondary SH2 Domain Binding Site, *Cell 138*, 514-524.
5. Otwinowski, Z., and Minor, W. (1997) Processing of X-ray diffraction data collected in oscillation mode, *Macromol Crystallogr, Pt A 276*, 307-326.
6. Adams, P. D., Grosse-Kunstleve, R. W., Hung, L. W., Ioerger, T. R., McCoy, A. J., Moriarty, N. W., Read, R. J., Sacchettini, J. C., Sauter, N. K., and Terwilliger, T. C. (2002) PHENIX: building new software for automated crystallographic structure determination, *Acta Crystallogr. D Biol. Crystallogr. 58*, 1948-1954.
7. Emsley, P., and Cowtan, K. (2004) Coot: model-building tools for molecular graphics, *Acta Crystallogr. D Biol. Crystallogr. 60*, 2126-2132.

8. Kabsch, W. (1976) Solution for Best Rotation to Relate 2 Sets of Vectors, *Acta Crystallogr A 32*, 922-923.

9. (1994) The CCP4 suite: programs for protein crystallography, *Acta Crystallogr. D Biol. Crystallogr. 50*, 760-763.

10. DeLano, W. L. (2002) The PyMOL User's Manual, *DeLano Scientific, San Carlos*.